doi: 10.15407/ujpe60.06.0511

A.A. EFREMOV, V.G. LITOVCHENKO, V.P. MELNIK, O.S. OBEREMOK,
V.G. POPOV, B.M. ROMANYUK

V.E. Lashkaryov Institute of Semiconductor Physics, Nat. Acad. of Sci. of Ukraine
(41, Prosp. Nauky, Kyiv 03628, Ukraine; e-mail: romb@isp.kiev.ua)

PACS 68.49.Sf, 82.80.Ms

MECHANISMS OF DOPANT DEPTH PROFILE MODIFICATION DURING MASS SPECTROMETRIC ANALYSIS OF MULTILAYER NANOSTRUCTURES

Mechanisms of the spatial redistribution of components in a solid target at its ion bombardment have been analyzed theoretically. The influence of the ion mixing, crater shape, and surface roughness on the results of mass spectrometric measurements is simulated as a function of the ion energy. All the above-mentioned factors are shown to have a minimal impact on the sputtering of nano-sized Mo/Si multilayer periodic structures in the ion energy interval of 200–400 eV. Experimental studies of the dopant depth profiles and their comparison with simulation results allowed us to establish the optimum conditions for the mass spectrometric analysis and to measure the real dopant depth profiles with a depth resolution better than 1 nm.

Keywords: simulation, sputtering, multilayer structure, depth profile, mass spectrometry.

1. Introduction

Mass spectrometry is widely used to make the elemental analysis of solid-state structures and materials [1, 2]. Owing to a high elemental sensitivity (up to 1×10^{13} cm^{-3}) and a high detection threshold with respect to the analyzed thickness equal to a few monolayers [3], the time-of-flight secondary ion mass spectrometry (ToF-SIMS) and the classical secondary ion mass spectrometry (SIMS) together with the neutral particle mass spectrometry (NPMS) remain to be the leaders in the elemental analysis of the surface and the bulk in semiconductor industry. In addition, the indicated methods make it possible to carry out a layer-by-layer analysis of multilayer structures consisting of different phases with a nanometer resolution over the specimen depth.

The analysis of the surface layer, as well as the removal of the latter in the course of the level-by-level analysis, is usually performed, by using the ionic sputtering. In this case, in addition to the direct sputtering of the target surface layers, the primary ions penetrate into the target depth. As a result, a large number of defect arise, and the spatial distribution of components in the target is strongly changed (ion beam mixing) even before the start of the direct mass spectrometric analysis of the corresponding layer [4].

Besides the mixing, the following main mechanisms of target transformation that affect the results of the mass spectrometric analysis can be mentioned: the formation of a statistical nanorelief in the course of sputtering (the surface roughness) [5], the formation of a macrocrater, whose surface becomes nonplanar, as the sputtering time grows (the "crater effect") [6], and the preferential sputtering of one of the target components [7]. An account and a minimization of the influence of those factors enable the information concerning the element composition to be obtained, in particular, the distribution profiles of impurities, which are as much close to the real ones as possible. This information is very important for the quan-

© A.A. EFREMOV, V.G. LITOVCHENKO, V.P. MELNIK, O.S. OBEREMOK, V.G. POPOV, B.M. ROMANYUK, 2015

titative researches carried out on the surface [8, 9], in the thin near-surface films [10], buried layers [11], periodic structures and superlattices [12, 13], as well as while studying such physical effects as the diffusion, segregation, and precipitation of impurities, and the formation and the decomposition of new phases in the solid [14–16].

When the multilayer nanostructures with the thickness of every layer equal to tens or less of nanometers are analyzed, the determination of the element composition distribution over the specimen depth (profiling) remains an extremely complicated diagnostic problem. The level-by-level analysis becomes even more complicated, if the layers are characterized by a certain (often unknown beforehand) structure that generates an additional nanoroughness of interphase boundaries, as well as if the intermetallic compounds and/or oxides are formed at the phase interfaces and on the specimen surface.

In this work, it is shown that a comprehensive analysis involving the influence produced by the ion beam mixing and "crater" effects and the development of a surface relief allows the regimes of mass spectrometry researches to be optimized, the resolution of the method over the specimen depth to be considerably improved, and the impurity distribution profiles, which are as much close to real ones as possible, to be obtained.

2. Theoretical Analysis of Factors Distorting the Impurity Distribution Profiles

2.1. Ion beam mixing processes

Penetrating into a solid, a high-energy primary ion loses its energy by means of a series of primary collisions and generates a cascade of high-energy secondary recoil atoms of the matrix. Those atoms, in turn, form the further fluxes of slower and slower particles until the ultimate stop of their motion. As a result of such cascade energy distribution, there emerges an inhomogeneous region in a vicinity of the primary ion trajectory, which is saturated with atoms shifted in various directions from their initial positions [17]. In this case, we may talk about the mixing of atoms associated with binary collisions. The vertical component of such atomic displacements is responsible for a smearing of interphase boundaries observed at the level-by-level analysis.

Characteristic threshold energies E_{th}^{lr} for some primary ions and recoil cascade atoms

Element	^{28}Si	^{16}O	^{96}Mo	^{40}Ar	^{84}Kr
E_{th}^{lr}, eV	40.95	23.40	140.41	58.50	122.86

When the surface is sputtered by low-energy primary ions, there exists a characteristic threshold energy, below which multiparticle collisions start to dominate over binary ones. In Table, the characteristic threshold energies E_{th}^{lr}, below which this transition takes place, are quoted for a number of primary ions and cascade recoil atoms [18]. The quoted values do not depend on the target material, which follows from the choice of a multiparticle interaction potential. The influence of the target is taken into account in the threshold energy values for target components, which determine the interaction for every collision cascade.

From the tabulated data, it follows that if the primary ion energy for the majority of primary recoil atoms equals several hundreds of electronvolts, their further collisions have a multiparticle character. In this interval of interaction energies between the primary ion and the target atom, not every collision results in an atom displacement. Even before the ion closely approaches the surface, a point-like influence on a certain site starts to be damped down by its nearest neighbors. Long-range forces and the bond deformation give rise to a situation where a whole group of atoms in a close vicinity to the given site starts to move more or less synchronously. As a result, the transferred energy is redistributed within a certain local block of the material without atomic shifts. As was already indicated, in the presence of regular atomic planes, such collective interaction leads to the reflection of incident particle backward. However, if there are vacancies in a vicinity of the knocked-out atom site, the atoms become partially isolated from their neighbors, which weakens the collective character of the interaction, and the medium ceases to behave as a massive reflector. The appearance of vacancies allows the atom to jump from its initial position avoiding a substantial deformation, environment reconstruction, and resistance of the medium.

Using the ionic-covalent materials with a large binding energy as an example, it is also demonstrated that the long-range potentials promote the influence of soft subthreshold collisions with a large impact pa-

rameter without displacements of atoms. Unlike the previous case, the subthreshold energy $E_{\rm th}^{\rm sub}$ is proportional here to the energy of an atom displacement from the site, E_d. The energy losses of a moving particle substantially decrease at that, being accumulated in the vibrational subsystem [19].

In order to calculate the ion beam mixing at low energies, we applied a phenomenological approach, in which the form of equations and the velocity coefficients made allowance for the following features revealed earlier with the use of the method of molecular dynamics: 1) a collective character of the interaction between a rapid particle and the medium and 2) the influence of the ordering in the atomic arrangement on the result of every separate collision, including the effect of reflection by the atomic layer. We assumed that an atom, even knocked out in a hard collision, cannot transit into the neighbor layer if there are no vacant places in the latter (the atom will be reflected backward). This model automatically considers a number of spillover effects, such as a small probability of the forward scattering and a prevailing localization of vacancies in the upper monolayer.

Let us consider the target as a set of atomic layers. The key parameters of the model are the probabilities of separate atom transitions–forward (into the solid depth, downward), $w_{j\to j+1} = d_j$; and backward (outside, upward), $w_{j\to j-1} = u_j$–for every j-th atomic layer involved in the mixing. Let $N_{\rm at} = \Omega^{-1}$ and $N_S = N_{\rm at}\lambda$ denote the bulk and surface, respectively, concentrations of atoms in the initial matrix, where λ is the interplane distance, and Ω the atomic volume. The current surface concentration for the j-th monolayer, N_S^j, can be presented in terms of the occupation degree $n_j(t)$ as follows:

$$N_S^j = n_j(t) N_S. \tag{1}$$

The balance equations for the kinetics of relative concentrations of atoms n_j in the layer and the vacancy fraction $V_j = 1 - n_j$ look like

$$\frac{d}{dt} n_1 = -(u_1 + V_2 d_1) n_1 + n_2 u_2 V_1 - f_1 n_1, \tag{2}$$

$$\frac{d}{dt} n_j = -(V_{j-1} u_j + V_{j+1} d_j) n_j + \big(n_{j+1} u_{j+1} + n_{j-1} d_{j-1}\big) V_j - f_j n_j. \tag{3}$$

Here, the first term describes the transitions of atoms from the given layer onto vacant places in the neighbor layers, the second one describes the arrival of atoms from the neighbor layers onto vacancies in the given layer, and the third one corresponds to the generation of noncompensated vacancies at the primary ion braking. This quantity depends on the number of hard collisions f_j per unit path of a primary ion, which is also proportional to the number of main atoms in the crystal lattice.

Owing to the sputtering in the vacuum, the first (top) monolayer permanently loses atoms and is enriched with mobile vacancies. The latter are filled with atoms arriving from the second and deeper layers. Hence, vacancies partially penetrate into the matrix.

The characteristic time needed to remove one monolayer, Δt, depends of the sputtering rate V_S and equals $\Delta t = \lambda / V_S$, where $\lambda \approx \sqrt[3]{\Omega}$. The sputtering process itself proceeds with the change in the layer enumeration, $n_1 \leftarrow n_2 \leftarrow n_3 \ldots n_j \leftarrow n_{j+1}$, the latter taking place, when the next portion of N_S atoms from the first layer transits into the vacuum.

While calculating the coefficients d_j and u_j in the equations, the experimental dependences of the sputtering rate on the primary ion energy, $V_S(E)$ [17], are used. The sputtering rate depends on the flux density J, concentration of impurity atoms, and sputtering coefficient S (the number of sputtered atoms per one primary ion):

$$V_S = J \Omega S. \tag{4}$$

The sputtering rate determines the scale of the coefficients $\{u_j\} = u_1 u_2 \ldots u_j$. It is easy to show that

$$u_1 = \frac{V_S}{\lambda} = \frac{1}{\Delta t} = \frac{J}{N_S} S. \tag{5}$$

The spatial density of primary ion energy losses determines the set of coefficients $\{d_j\}$, which are proportional to the intensities of atomic jumps forward, provided that the population degree of the given j-th layer equals unity, and the $(j+1)$-th layer is completely vacant. It can be presented in the form

$$d_j = k \xi \beta J \frac{E_j}{2E_d}, \tag{6}$$

where $\xi < 1$ is a correction for the collision softness ($\xi \approx 0.8$), E_j is the energy of the ion entering the j-th layer (E_1 is the energy of the primary ion), E_d the energy of an atom displacement from the site, the coefficient $\beta = 1/4 \div 1/2$ characterizes the fraction of

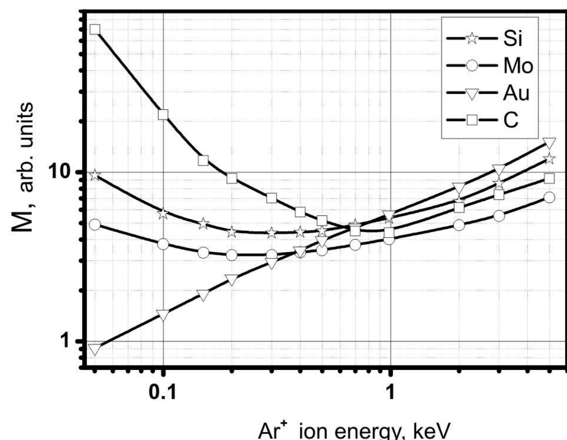

Fig. 1. Calculated dependences of the mixing effect on the energy of bombarding argon ions for atomic layers of different types

atoms knocked out forward, and k has the dimensionality of area.

A similar estimation, but with a different coefficient, is also valid for the rate constants $\{u_j\}$:

$$u_j = k\xi(1-\beta)J\frac{E_j}{2E_d}. \quad (7)$$

Knowing the probabilities of atomic transitions into the lower and upper atomic planes in the solid, we can evaluate the magnitude of ion beam mixing depending on the ionic sputtering energy, which allows us to determine the optimum sputtering energy with the smallest influence of the mixing effect on the profiles of the impurity distribution over the depth. In Fig. 1, the normalized (for an ion energy of 0.5 keV) dependences of the parameter M that characterizes the mixing degree in deep layers of silicon, carbon, gold, and molybdenum on the energy of sputtering argon ions are depicted. This parameter was calculated as the number of recoil atoms per one sputtered atom of the target. It is evident that the character of this dependence is substantially different for different targets.

In particular, in the case of gold, the minimum mixing effect is observed at low energies, whereas those energies correspond to the mixing maximum in the case of carbon. Hence, in order to reduce the ion beam mixing effect at the profiling of multicomponent and/or multilayer structures, it is necessary to choose such sputtering energy, at which the parameter M is minimum for the majority of impurities actual for researches. For silicon and molybdenum, the minimum value of the parameter M is observed near energy values of 220 and 300 eV, respectively. Therefore, the mass spectroscopic analysis of periodic Mo/Si structures was carried out, by using the argon sputtering ions with energies in the interval of 200–450 eV.

2.2. Influence of a statistical nanorelief

As the first approximation, the neighbor atoms are considered to be sputtered independently of one another. As a result, there arise the neighbor nano-sized dips and humps that evolve also independently. The simplest stochastic theory of this effect [21] shows that the characteristic amplitude of a nanorelief h_m should gradually grow in time following the law $\sqrt{t}$, and the distribution function of relief heights should be described by a Gaussian. However, there are a number of factors that counteract the unconfined growth of nano-roughnesses. These are the diffusion along the surface with a varying curvature and the resputtering, i.e. when the substance sputtered from the lateral slopes of the relief humps is partially accumulated in the relief dips. The both mechanisms result in that the high-frequency harmonics become smoothed out first of all, whereas a certain stationary low-frequency relief survives. If the distribution function of relief heights equals $\varphi(h,t)$ at the moment of sputtering, the registered profile $\Pi(t)$ of a definite component will look like

$$\Pi(t) = \int\limits_{-h_m}^{+h_m} \varphi(h,t)F(z+h)dh. \quad (8)$$

Here, $z(t) = \int_0^t v_s(\tau)d\tau$ is the average depth of the sputtered surface reached by the time moment t, $F(x)$ is the actual component distribution over the depth, v_s the instant sputtering rate, and $\pm h_m$ the maximum relief amplitude at the time t.

In the framework of the simplest stochastic theory, the function $\varphi(h,t)$ is described by a Gaussian distribution. It is clear that the profile smearing at the interphase boundaries is given by the quantity $\pm h_m$. Figure 2 exhibits the data obtained for a distortion of the initial profile at the sputtering of the multilayer target owing to the development of a statistical relief with the amplitude growing proportionally to $\sqrt{t}$. One can see that the sinusoidal smearing

of rectangular concentration pulses takes place, and their amplitudes gradually decrease.

The low-energy ionic bombardment (<400 eV) has a certain specific character in the processes of surface relief formation. Here, a number of new effects are observed, which are mainly associated with the surface localization of radiation-induced vacancies. The latter not only actively dissolve the relief humps, but also smooth the relief [22] as a result of the ion-stimulated surface diffusion. At the same time, it was shown [23] that the application of sputtering ions with energies lower than 100–150 eV brings about a drastic growth of the surface roughness. Hence, in order to obtain a high resolution over the depth, ions with higher energies have to be used.

2.3. Crater effect

In the course of target sputtering by ions, there emerges a crater, the bottom of which can be non-planar, i.e. it can be concave or convex, with its curvature, as a rule, gradually growing, as the sputtering time increases. In this case, the contributions to the measured signal are given by the crater surface sections, whose compositions correspond to different depths of the initial specimen. Therefore, the measured profile of the impurity distribution over the depth depends on crater's bottom shape and its variation in time.

In a simple case, crater's bottom can be approximated as a concave spherical segment with the base radius a (the collection region of analyzed particles), maximum depth H, and bottom curvature radius R (Fig. 3). Then we have

$$S_{\rm cr} = \pi a^2$$

for the base area and

$$S = S(R,H) = 2\pi RH = \pi(H^2+a^2) = S_{\rm cr}(1+\varepsilon^2) \quad (9)$$

for the area of crater's bottom. The curvature of crater's bottom $K = 1/R$ is given by the relation

$$K = \frac{2H}{H^2+a^2} = \frac{1}{a}\frac{2\varepsilon}{1+\varepsilon^2}, \quad (10)$$

where the quantity $\varepsilon = H/a$ characterizes a deviation of crater's bottom from the plane; in particular, $\varepsilon = 0$ in the plane case, and $\varepsilon = 1$ for a hemispherical crater. Let us estimate the influence of such crater on the measured profile shape.

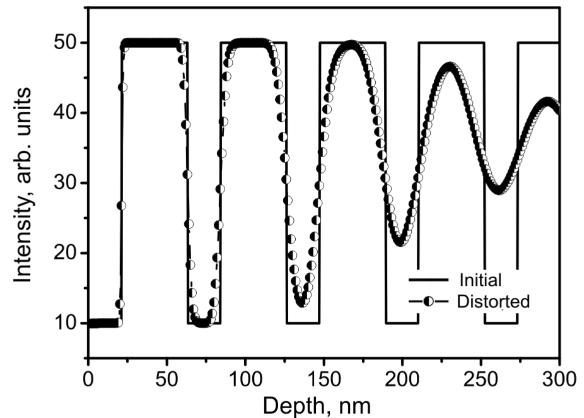

Fig. 2. Distortion of the initial profile at the sputtering of a multilayer target owing to the development of a statistical relief

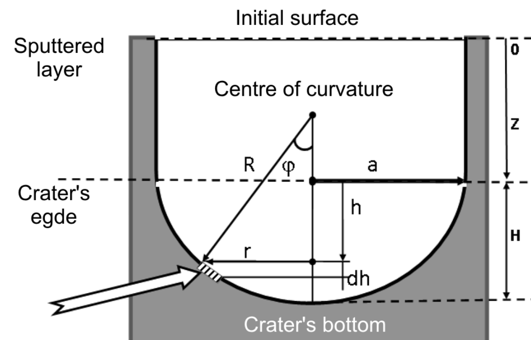

Fig. 3. Transverse cross-section of a specimen with a crater. The arrow points to in an elementary section of crater' bottom

Let the upper edge of the crater reach the level z in the initial specimen in the course of sputtering (Fig. 3). At this moment, all sections of the surface located below this level down to the depth $z+H$ give contributions to the detected signal. Let the notation $dS(h)$ stand for the elementary section area located at an intermediate depth $z+h$ $(0 \leqslant h \leqslant H)$. This depth is connected with the angle $\varphi = \varphi(h)$ between the normal to the specimen plane and the local normal to the crater surface. The quantity $\cos\varphi = (R-H+h)/R$ determines the fraction of the flux of secondary particles arrived at the collecting system. The quantity $\frac{dS(h)}{S(R,H)}$ plays the role of a distribution function for sections with different compositions simultaneously giving a contribution to the measured signal. Then the expression for the resulting profile

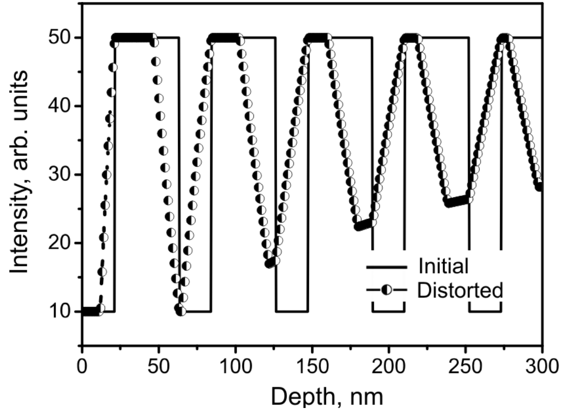

Fig. 4. Distortion of the initial profile at the sputtering of a multilayer target owing to the crater effect

looks like

$$\Pi(z)=\int_0^S \frac{dS(h)}{S(R,H)}F(z+h)\cos\varphi(h). \qquad (11)$$

Here, the integration is carried out over the whole area of crater's bottom, which is simulated as a spherical segment. The elementary section dS (Fig. 2) corresponds to a ring located on the spherical surface at the depth h and is characterized by the width $Rd\varphi$ and the radius $r=R\sin\varphi$:

$$dS(h)=2\pi R^2\sin\varphi d\varphi, \qquad (12)$$

$$\Pi(z)=\frac{R}{H}\int_0^\Phi F(z+h(\varphi))\sin\varphi\cos\varphi d\varphi, \qquad (13)$$

$$h(\varphi)=H-R(1-\cos\varphi), \quad \Phi=\arcsin(a/R). \qquad (14)$$

In the general case of an arbitrary initial profile, it is more convenient to calculate the integral on the right-hand side of Eq. (13) numerically.

Since the slow primary ions are more sensitive to a planar nonuniformity of the electric field around the specimen and to the aberrations in ion optics, their usage, provided that other conditions are identical, should result in a more pronounced crater effect, than in the case of primary ions with higher energies. Figure 4 illustrates the distortion of the initial profile at the sputtering of a multilayer target as a result of the crater development, when the crater depth grows proportionally to $\sqrt{t}$, since $\sqrt{d}=\sqrt{V_S t}$. One can see a characteristic saw-like distortion of the rectangular concentration pulses, which is different from the statistical relief (Fig. 2). In this case, the minimum impurity concentration for deeper layers gradually increases. Hence, the problem of crater effect elimination remains to be the most important for the level-by-level analysis of nano-sized layered structures.

2.4. Preferential sputtering of certain components

On the surfaces and at the interphase boundaries of layered structures, the intermetalloids and the oxides of complex compounds can be formed. Let us demonstrate that the analysis of secondary neutrals allows the composition of those regions to be adequately analyzed despite the possible selective sputtering effect. Let us consider a bulk phase with the composition AB_n. When the surface is sputtered, the fluxes of atoms of each kind, $J_{A,B}$, can be expressed in terms of the surface concentrations $N_S^{A,B}$ and the partial sputtering coefficients $k_{A,B}$ in the form

$$J_A=k_A N_S^A, \quad J_B=k_B N_S^B.$$

First, let the surface stoichiometry corresponds to the bulk one, i.e. $N_S^B/N_S^A=n$. The preferential sputtering means that either of the components (e.g., B) can be emitted more intensively than the other one, i.e. $k_B>k_A$. At the initial moment, the flux of atoms B is higher, so that their surface concentration will decrease to a new stationary value $\langle N_S^B\rangle$, which is k_B/k_A times as low as the initial one. The stationary flux of component B will now be determined by the relation

$$J_B=k_B\langle N_S^B\rangle=k_B N_S^B\frac{k_A}{k_B}=k_A N_S^B.$$

Hence, the ratio between the fluxes in the stationary regime equals the ratio between the bulk concentrations, $J_B/J_A=N_S^B/N_S^A$, which is evident, if we proceed from the substance conservation law: "Everything sputtered has been analyzed". Hence, in the case of secondary post-ionized neutral particles, the selectivity of the sputtering does not affect the registered signal. This is a principal advantage of this method in comparison with the Auger electron spectroscopy and, partially, SIMS. For the latter, the probability of the secondary particle ionization can also depend on the nearest environment in the matrix, which, under the conditions of the preferential sputtering for the bulk and the surface, turns out different.

3. Experimental Technique and Research Object

Multilayer periodic coatings (MPCs) were fabricated using the method of sequential magnetron sputtering of molybdenum and silicon layers. The magnetron currents and the argon pressure in the chamber were maintained constant, which provided a steady rate of layer deposition. The deposition rate of molybdenum was constant, while fabricating all MPCs, and equal to about 0.312 nm/s. The deposition rate of silicon changed from 0.35 to 0.45 nm/s depending on the magnetron discharge current. Multilayer coatings were deposited onto silicon substrates with a surface roughness of 0.3–0.5 nm. Molybdenum and silicon wafers of 99.5 and 99.99% purity, respectively, were used as target ones.

NPMS measurements of the impurity distributions over the depth of multilayer Mo/Si structures were performed on a Laybold-Heraeus INA-3 device in the regime of high-frequency (HF) sputtering by low-energy Ar^+ ions (the energy $E_{Ar^+} = 200 \div 450$ eV) of a low-pressure plasma (3.26×10^{-3} mbar). The ions were generated by applying the accelerating voltage in the form of rectangular pulses with the negative polarity, a frequency of 50 kHz, and a pulse ratio of 0.6 to the specimen. The sputtering region was confined by means of tantalum diaphragms with internal diameters varying from 1.5 to 3 mm. The shape of the crater and its depth were estimated with the use of a DEKTAK 3030 stylus profilometer.

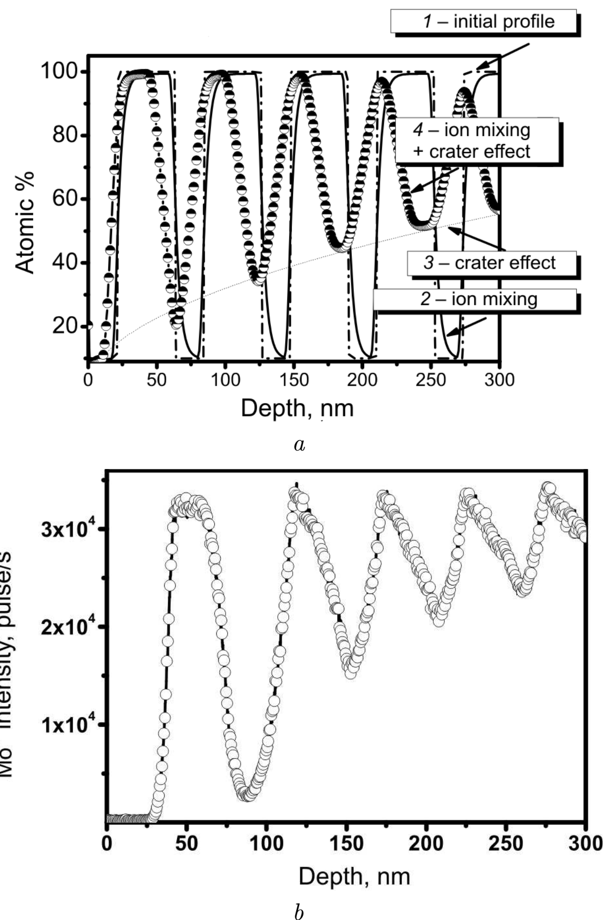

Fig. 5. Calculated (*a*) and experimental (*b*) profiles of the Mo distribution at the sputtering of a multilayer Mo–Si target

4. Comparison of Theoretical and Experimental Results

In Fig. 5, the theoretical (*a*) and experimental (*b*) profiles of the molybdenum distribution in a multilayer Mo/Si structure are shown. The calculations demonstrate that, when the first layer of a multilayer periodic structure is sputtered, a distortion of the rectangular Mo concentration distribution characteristic of the ion beam mixing is observed. The further sputtering results in a saw-like distortion of the profile owing to the combined action of the ion beam mixing and the crater effect. The concentration oscillation minima gradually grow at that. The comparison of the theoretically calculated Mo distribution profiles (Fig. 5, *a*) and the experimental results of the NPMS analysis (Fig. 5, *b*) testifies to rather a good agreement between them.

In Fig. 6, the Si distribution profiles obtained at sputtering a Mo/Si structure, by using Ar^+ ions in the examined energy interval, are depicted. Every profile demonstrates a characteristic growth of the signal intensity in the course of sputtering and a simultaneous growth of the signal intensity minimum at the sites, where molybdenum layers are located (Fig. 7). According to the results of theoretical calculations, such behavior of the profiles is associated with the influence of the crater effect on the sputtering process.

The results of simulation (Fig. 5, *a*) reveal that, starting from a certain time moment t_0, the dependence of the quasi-spherical crater depth H on the sputtering time can be described by the relation $H = \alpha' \sqrt{t - t_0}$ or $H = \alpha \sqrt{d - d_0}$, where d is the thickness of the layer sputtered by the time t. The

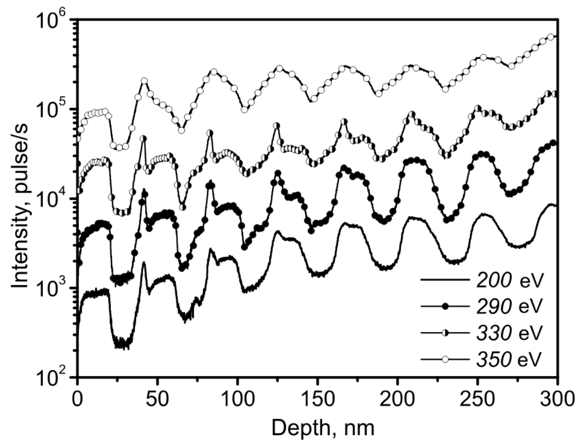

Fig. 6. Distribution profiles of the Si impurity in a Mo/Si multilayer structure for various energies of primary ions

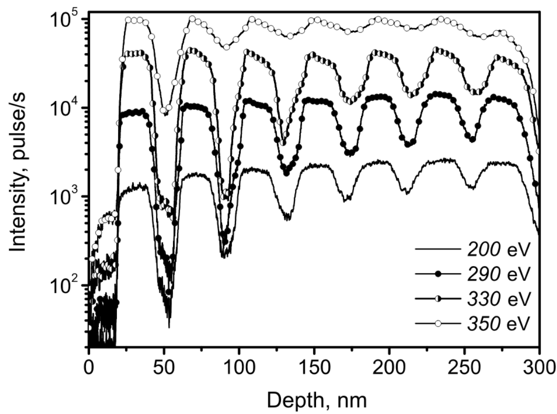

Fig. 7. Distribution profiles of the Mo impurity in a Mo/Si multilayer structure for various energies of primary ions

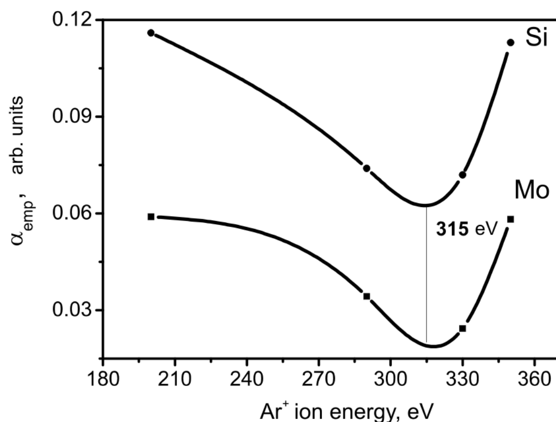

Fig. 8. Dependences of the empirical coefficient of crater formation on the bombardment energy

minima of the registered profile in the layered system trace the indicated root dependence. The coefficient α can be naturally called the crater formation intensity. The corresponding curve $I = a\sqrt{d - d_0}$ is the lower directrix for the profile of the secondary particle yield intensity, and the coefficient a is proportional to α. We used this approximation of experimental data in Figs. 6 and 7 to calculate the empirical coefficient of crater formation $\alpha_{\text{emp}} = a/I_1$, where I_1 is the secondary particle yield at the first profile maximum not distorted by the crater.

The major cause of the "crater effect" emergence at the ion sputtering of the surface is connected with the lateral inhomogeneity of the ion beam. If the beam inhomogeneity should not change in time, the crater depth would increase linearly at a certain average rate. The fact that the crater effect manifests itself in the distribution profiles of periodic structures as the function $\sqrt{t}$ (Fig. 4) may testify to the influence of statistically independent processes occurring as a result of the ionic bombardment. The observed dependence means that the beam density fluctuates. The sections sputtered more intensively at a certain time moment (e.g., the central part of the specimen or its periphery) become less exposed at the next time moments and *vice versa*. As a result, the sections that are located closer to the initial (before the sputtering began) surface permanently exchange their positions with the sections located more deeply. Such behavior of physical systems, when their evolution is governed by random transitions between closely located states, is widely spread in the nature, in particular, at the excitation of atoms in low-temperature plasma, ion mixing in a solid, formation of a statistical nanorelief at the surface sputtering, and so on.

The time fluctuations in a primary ion beam can be observed experimentally during the multilayer specimen sputtering. They result from both the instability of the equipment working parameters (according to the technical certificate of our installation, it was lower than 3%) and the specific features of the ion sputtering for different materials (dielectric, metallic, *etc.*) In particular, changing from metallic layers to semiconductor or dielectric ones can lead to the defocusing of the ion beam and/or a change in the ion flux density.

The normalization procedure makes it possible to compare the crater formation in various specimens under various sputtering conditions on the basis of

measured profiles only. In Fig. 8, the corresponding dependences of the empirical coefficient of crater formation on the bombardment energy calculated in the interval from 200 to 350 eV are exhibited. The calculations, which were carried out for silicon (Fig. 6) and molybdenum (Fig. 7) profiles, brought about similar results. The analysis of experimental dependences allowed us to revealed the obscured minimum at about 314–319 eV in both dependences. It is this interval of primary ion energies, where the crater effect should expectedly have the minimum influence on the impurity distribution profiles in layered periodic structures.

The presented results testify that, if a multilayer Mo/Si structure is sputtered with the use of low-energy argon ions, there exists an energy interval (290–310 eV), in which the crater effect is minimal.

5. Conclusions

A statistical theory is developed, and a detailed analysis is carried out concerning the mechanisms of distortion of the impurity distribution profiles at the low-energy NPMS analysis of multilayer nano-sized periodic coatings. The influence of the ion beam mixing, sputtering crater shape, and surface roughness on the results of mass spectrometric measurements and its dependence on the energy of sputtering ions are calculated. The optimum range for the latter is found to be 290–310 eV, which allows the impurity distribution profiles in periodic structures to be measured with the minimum influence of distortion factors.

To compare our theoretical calculations with the experimental results, the sputtering of multilayer nano-sized periodic structures is studied, by using argon ions with energies in an interval of 200–400 eV. The structures were fabricated by the sequential magnetron sputtering of molybdenum and silicon layers. The developed mathematical models describe well the real processes of interaction with low-energy ions and make it possible to calculate the impurity distribution profiles in multilayer periodic coatings, as well as to distinguish and to minimize the major factors giving rise to a profile distortion.

This work was supported in the framework of the State target-oriented scientific and technical program "Nanotechnologies and nanomaterials" in 2010–2014 (project 3.5.1.28) and the common scientific project of the NAS of Ukraine and the Russian Fund of Fundamental Researches in 2014 (project 76-02-14(U)).

1. R.G. Wilson, F.A. Stevie, and C.W. Magee, *Secondary Ion Mass Spectrometry: A Practical Handbook for Depth Profiling and Bulk Impurity Analysis* (Wiley, New York, 1989).
2. http://www.eag.com.
3. J.C. Vickerman and D. Briggs, *ToF-SIMS: Surface Analysis by Mass Spectrometry* (IM Publications, Chichester, UK, 2001).
4. I.P. Lisovskii, V.G. Litovchenko, V.B. Lozinskii, and V.P. Melnik, Thin Solid Films **247**, 264 (1994).
5. F. Ludwig, C.R. Eddy, O. Malis, and R.L. Headrick, Appl. Phys. Lett. **81**, 2770 (2002).
6. E. Stumpe, H. Oechsner, and H. Schoof, Appl. Phys. **20**, 55 (1979).
7. S. Berg and I.V. Katardjiev, J. Vac. Sci. Technol. A **17**, 1916 (1999).
8. K.O. Butarev, I.P. Koval', Yu.A.Len', and M.G. Nakhodkin, Nano-Elektron. Fiz. **5**, 01025 (2013).
9. O. Oberemok and P. Lytvyn, Semicond. Phys. Quant. Electr. Optoelectr. **5**, 101 (2002).
10. A. Goriachko , P.V. Melnik, A. Shchyrba, S.P. Kulyk, and M.G. Nakhodkin, Surf. Sci. **605**, 1771 (2011).
11. V. Melnik, A. Misiuk, V. Popov, O. Oberemok, B. Romanyuk, D. Gamov, and P. Formanek, Ukr. J. Phys. **32**, 34 (2007).
12. V. Melnik, D. Wolanski, E. Bugiel, A. Goryachko, S. Chernjavski, and D. Kruger, Mater. Sci. Eng. B **102**, 358 (2003).
13. Yu.P. Pershin, V.A. Sevryukova, E.N. Zubarev, A.S. Oberemok, V.P. Melnik, B.N. Romanyuk, V.G. Popov, and P.M. Litvin, Metallofiz. Noveish. Tekhnol. **35**, 1617 (2013).
14. D. Kruger, H. Ruker, B. Heinemann, V. Melnik, R. Kurps, and D. Bolze, J. Vac. Sci. Technol. B **22**, 455 (2004).
15. A. Romanyuk, P. Oelhafen, R. Kurps, and V. Melnik, Appl. Phys. Lett. **90**, 013118 (2007).
16. D. Kruger, B. Romanyuk, V. Melnik, Ya. Olikh, and R. Kurps, J. Vac. Sci. Technol. B **20**, 1448 (2002).
17. R. Berish, *Sputtering by Particle Bombardment* (Springer, Berlin, 1981).
18. N.V. Kostina, Ph.D. thesis (Penza,2003) (in Russian).
19. A.A. Efremov, Ph.D. thesis (Kyiv, 1989) (in Russian).
20. E. Chason, P. Bedrossian, K.M. Horn, J.Y. Tsao, and S.T. Picraux, Appl. Phys. Lett. **57**, 1793 (1990).
21. P. Bedrossian, J.E. Houston, J.Y. Tsao, E. Chason, and S.T. Picraux, Phys. Rev. Lett. **67**, 124 (1991).
22. B. Poelsema, L.K. Verheij, and G. Comsa, Phys. Rev. Lett. **53**, 2500 (1984).
23. R. Čerapaitė-Trušinskienė, and A. Galdikas, Medžiagotyra **15**, 139 (2009).

Received 15.08.14.
Translated from Ukrainian by O.I. Voitenko

О.О. Єфремов, В.Г. Литовченко, В.П. Мельник,
О.С. Оберемок, В.Г. Попов, Б.М. Романюк

МЕХАНІЗМИ МОДИФІКАЦІЇ
ПРОФІЛІВ РОЗПОДІЛУ ДОМІШОК
ПРИ МАС-СПЕКТРОМЕТРИЧНОМУ АНАЛІЗІ
БАГАТОШАРОВИХ НАНОСТРУКТУР

Р е з ю м е

Проведено теоретичний аналіз механізмів, які приводять до просторового перерозподілу компонентів твердотільної мішені під дією іонного бомбардування. Виконано моделювання впливу іонно-променевого перемішування, форми кратера розпилення та шорсткості поверхні на результати мас-спектрометричних вимірювань залежно від енергії розпилюючих іонів. Показано, що в діапазоні енергій іонів 200–400 еВ вплив згаданих факторів є мінімальним для розпилення багатошарових нанорозмірних періодичних структур Mo/Si, виготовлених методом магнетронного напилення шарів молібдену і кремнію. Експериментальні дослідження профілів розподілу домішок і порівняння їх з результатами моделювання дозволило встановити оптимальні режими мас-спектрометричного аналізу, досягти роздільної здатності по глибині краще 1 нм та отримати профілі розподілу домішок, максимально наближені до реальних.